Hamiltonian transformation to compute Thermo-osmotic Forces

Raman Ganti,[1] Yawei Liu,[2] and Daan Frenkel[1,*]

[1] *Department of Chemistry, University of Cambridge, Lensfield Road, Cambridge CB2 1EW, UK*
[2] *Beijing University of Chemical Technology, Beijing, P. R. China*

(Dated: July 16, 2018)

If a thermal gradient is applied along a fluid-solid interface, the fluid experiences a thermo-osmotic force. In steady state this force is balanced by the gradient of the shear stress. Surprisingly, there appears to be no unique microscopic expression that can be used for computing the magnitude of the thermo-osmotic force.

Here we report how, by treating the mass M of the fluid particles as a tensor in the Hamiltonian, we can eliminate the balancing shear force in a non-equilibrium simulation and therefore compute the thermo-osmotic force at simple solid-fluid interfaces. We compare the non-equilibrium force measurement with estimates of the thermo-osmotic force based on computing gradients of the stress tensor. We find that the thermo-osmotic force as measured in our simulations cannot be derived from the most common microscopic definitions of the stress tensor.

Nanotechnology is not just conventional technology scaled down to the nano scale. The reason is that processes that are relatively unimportant on macroscopic scales may become dominant on the nano-scale. Case in point are phoretic flows: the movement of fluids under the influence of gradients of thermodynamic quantities such as temperature or chemical potential. On a macroscopic scale, the application of a pressure gradient or a body force is the most efficient way to move fluid through a tube. The resulting flux is proportional to the fourth power of the tube diameter. However, on a sub-micron scale, phoretic flows tend to become important because the resulting volumetric flow rates scale as the square of the tube diameter. Hence, for many problems, be they technological (e.g. nano-fluidics) or natural (e.g. fluid flow through porous networks or gels), it is becoming increasingly important to be able to predict phoretic flows.

A key feature of phoretic flows is that they are driven by forces that only act on those parts of the fluid that interact with the confining surfaces. The range of the fluid-wall interactions is typically in the nano-meter regime, except in the case of electrolytes in contact with charged surfaces, in which case the interaction layers may have thicknesses ranging from nanometers to microns. Here we will be considering thermo-osmotic forces in non-polar fluids near a wall. For such systems, the thermo-osmotic force driving the flow is typically confined to an interfacial layer with a thickness of a few molecular diameters. Thermo-osmotic flows have been known for well over a century [1, 2], but the relevance of this phenomenon is increasing as more experiments probe transport on the nano-scale. Moreover, there is increasing evidence that large temperature gradients may exist inside eukaryotic cells [3], which is also an environment full of interfaces.

Derjaguin [4] formulated a generic description of thermo-osmosis in the language of irreversible thermodynamics. As the approach by Derjaguin (and others) is phrased in the language of macroscopic thermodynamics and continuum hydrodynamics (creeping-flow equations), it cannot be used for a quantitative prediction of the magnitude of thermo-osmotic flows from knowledge of the intermolecular interactions. Moreover, the validity of continuum hydrodynamics is questionable in the first few molecular layers near a wall.

Yet, a microscopic implementation of Derjaguin's approach is possible by using the Onsager reciprocity relations to relate the flow due to a temperature gradient to the more easily calculated, excess heat flux due to a pressure gradient. In fact, in earlier work [5] we found reasonable agreement between the Onsager approach and non-equilibrium simulations. Fu, Merabia and Joly [6] also used the Onsager approach to estimate the thermo-osmosis coefficient near a water-graphene interface. However, neither our methods nor those developed in Ref. [6] allow us to compute directly the forces on a fluid due to thermal gradients parallel to a surface.

As noted by Anderson [7], the stress tensor, $\sigma_{\alpha\beta}$, near an interface is anisotropic. Force balance normal to the interface means that σ_{zz} is constant, whereas the transverse stress, σ_{xx}, will depend on z. A temperature gradient in the $x-$direction induces a local stress gradient parallel to the interface. The stress σ_{xx} depends on x only through its (explicit or implicit) dependence on temperature [5]:

$$\frac{\partial \sigma_{xx}(z)}{\partial x} = \left(\frac{\partial \sigma_{xx}(z)}{\partial T}\right)_{P_{\rm bulk}} \frac{\partial T}{\partial x}. \qquad (1)$$

The temperature derivative is computed at con-

stant bulk pressure because thermal gradients do not cause pressure gradients in the bulk of the liquid. Therefore, the dependence of σ_{xx} on T will vanish in the bulk. As temperature is the only quantity that is varied, the local stress gradient must originate from intermolecular forces.

Here we use molecular simulations to predict the strength of the local stress gradient. The most straightforward approach is to carry out non-equilibrium Molecular Dynamics simulations to probe thermally induced forces. However, explicitly imposing a thermal gradient cannot work, because in steady-state the net force on all fluid particles must necessarily vanish: the flow induced by the local stress gradient causes a gradient in shear stress [7] that cancels the thermo-osmotic force (Eq. (1)) (see SM: Non-equilibrium Method):

$$\frac{\partial \sigma_{xz}(z)}{\partial z} = -\frac{\partial \sigma_{xx}(z)}{\partial x}. \tag{2}$$

Because the viscous shear force is directly proportional to the fluid velocity, eliminating flow should cause it to vanish so that only the local stress gradient remains. As we will later show, the simplest way to accomplish this is to treat the mass M of the fluid particles as a tensor in the Hamiltonian, and consider the limit where $M_{yy} = M_{zz} = M$, the original mass of the particles, whilst $M_{xx} \to \infty$. As the kinetic energy remains finite, $v_x \to 0$ for all fluid atoms thereby eliminating the shear force.

To gain insight on the microscopic origins of the thermo-osmotic force, it is necessary to isolate the forces due to the thermal gradients from those due to gradients in the shear stress. The normal route to obtain the force $f_x^V(z)$ on a volume element in a liquid is to compute the gradient of stress acting on that element. Here z denotes the distance from the interface, and x the direction of the force parallel to the wall. The superscript V indicates that $f_x^V(z)$ is the force per unit volume. We can convert $f_x^V(z)$ into $f_x^P(z)$, the force per particle, by using $\rho(z) f_x^P(z) = f_x^V(z)$, where $\rho(z)$ is the number density at a distance z from the wall.

Eq. (1) provides a convenient route to compute stress gradients numerically, because the temperature dependence of the stress tensor can be computed from equilibrium simulations at slightly different temperatures by numerical differentiation:

$$\frac{\partial \sigma_{xx}(z)}{\partial T} \approx \frac{\sigma_{xx}^{eq,T_2}(z) - \sigma_{xx}^{eq,T_1}(z)}{T_2 - T_1}. \tag{3}$$

In what follows, we denote the approach based on Eqs. (1) and (3) as the "stress-gradient" route (see SM: Stress Gradient Method). The stress-gradient method would seem to offer a route to compute phoretic forces in thin layers from the microscopic definition of the stress tensor. However, as we show below, this approach fails. We recall that the definition of the microscopic stress tensor is not unique. This ambiguity is not a problem when computing the bulk pressure, or even the surface tension [8]. However, for stress gradients parallel to a surface, different definitions of the microscopic stress do not yield the same answer. The obvious question is then: which stress tensor provides the correct description. The surprising answer that we find is "none" (at least not one of the usual suspects).

As an alternative to computing the microscopic stress gradient, we can relate the gradient of the position-dependent stress to the local value of the excess enthalpy [5] (see SM: Local Thermal Equilibrium (LTE) Method for derivation):

$$\frac{\partial \sigma_{xx}(z)}{\partial x} = -\left(\frac{\Delta h(z)}{T}\right)\frac{\partial T}{\partial x} \tag{4}$$

where $\Delta h(z)$ is the excess enthalpy density. Note that Eq. (4) can be obtained from a single equilibrium simulation.

Due to the non-uniqueness of the definition of the stress tensor, different definitions may yield different stress gradients. The most commonly used microscopic stress definitions are the virial (V) (see e.g. [9]) and the Irving-Kirkwood (IK) [10]. Both definitions have identical kinetic (K) contributions ($\sigma_{xx}^K(z) = -\rho(z) k_B T$). The non-uniqueness of the stress arises from different definitions of the potential (ϕ) stress (see SM: Stress-Gradient Method).

Therefore, Eqs. (3) and (4) provide at least three distinct expressions for the thermo-osmotic force. We can evaluate Eq. (1) using both stress expressions in Eq. (3) and compute Eq. (4) via our local thermodynamic expression for $\Delta h(z)$ (Eq. S(23)). Then, the thermo-osmotic force per particle is given by

$$f_x^P(z) = \frac{1}{\rho_{ave}(z)}\left(\frac{\partial \sigma_{xx}(z)}{\partial x}\right) \tag{5}$$

where $\rho_{ave}(z) = (\rho(T_1, P, z) + \rho(T_2, P, z))/2$.

As the three methods for evaluating the thermo-osmotic force give different answers (see Fig 2), we would like to know which, if any of these, is correct. The obvious approach is to compute the thermo-osmotic force in a steady-state, non-equilibrium simulation. To eliminate the shear stress (Eq. (2)) in a non-equilibrium simulation, so that only the thermo-osmotic force remains, we propose the following non-equilibrium simulation technique: First, we impose a

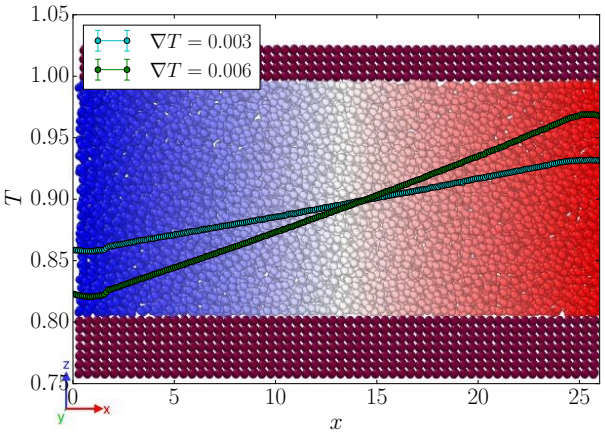

FIG. 1: Simulation box used for non-equilibrium force calculation. Fluid atoms (blue, white, and red) interact with solid atoms (maroon) bonded together via harmonic springs. Temperature profiles are plotted over the simulation box and the color gradient indicates a gradual progression from cold to hot atoms.

periodic temperature gradient along x. This is done by selecting the left-most part of the simulation box (see Fig S2 in SM) and thermostatting at a temperature lower than the average ($T = 0.9$) while also selecting the middle of the simulation box and thermostatting at a temperature higher than the average (see SM: Non-equilibrium Method). The resulting heat current sets up the thermal gradient.

After the system has reached steady-state, we change the equations of motion for the fluid atoms: in particular, we now treat the mass M of the fluid particles as a tensor in the Hamiltonian, and consider the limit where $M_{xx} \to \infty$. Transforming the Hamiltonian in this way changes the dynamics of the system, but static properties such as inter-molecular interactions remain the same. Equipartition would still hold in this model system: hence, the average kinetic energy associated with motion in the x direction is still $k_BT/2$. As

$$v_x = \sqrt{\frac{k_BT}{M_{xx}}}, \tag{6}$$

$v_x \to 0$ for all fluid atoms. Since M_{yy} and M_{zz} are still equal to M, the original mass of the particles, fluid atoms are still diffusing in the y and z directions. As the average kinetic energy does not change, the magnitude of the temperature gradient is left unchanged (Fig 1). In other words, we have switched off the shear flow, whilst maintaining the temperature gradient (see SM: Non-equilibrium Method).

In this stationary system, the bulk serves as a reservoir of atoms so that fluid near the surface can rearrange to the local-equilibrium density profile. As the gradient in shear stress $\partial\sigma_{xz}(z)/\partial z$ now vanishes, only the thermo-osmotic force will remain. To compute the average thermo-osmotic force, we must average the per-atom force calculation over many different initial configurations, as every single realization will have a different density-profile in the x-direction frozen in.

In our numerical calculations, we consider a Lennard-Jones fluid consisting of $N = 7920$ atoms interacting via a truncated and shifted Lennard-Jones potential

$$V_{\text{trunc}}(r) = \begin{cases} 4\epsilon\left[\left(\frac{\sigma}{r}\right)^{12} - \left(\frac{\sigma}{r}\right)^{6}\right] - V(r_c) & r \le r_c \\ 0 & r > r_c. \end{cases} \tag{7}$$

where $r_c = 4\sigma$. In what follows σ is our unit of length and ϵ is our unit of energy: all computed quantities are expressed in reduced units. We carried out simulations where this fluid was in contact with three different surfaces: a structured wall interacting with fluid through a less attractive Lennard-Jones potential, a structured wall interacting via a purely repulsive Weeks-Chandler-Andersen (WCA) potential [11], and a reflecting wall that simply flips the corresponding velocity of fluid atoms if they attempt to cross it. The parameters for interaction between the fluid and structured wall are: $\sigma_{\text{fluid-fluid}} = \sigma_{\text{solid-fluid}} = \sigma$. The interaction strength between the fluid and structured wall is given by $\epsilon_{\text{solid-fluid}} = 0.55\epsilon$. The WCA interaction between the fluid and repulsive wall atoms was obtained by truncating and shifting the fluid-fluid interaction at $r_c = 2^{1/6}\sigma$.

All Molecular Dynamics simulations were carried out using the LAMMPS package [12]. Fig 1 shows a simulation cell of length $\langle L_x\rangle = 49.32\sigma$ and $\langle L_y\rangle = 9.86\sigma$ containing fluid that interacts with a structured wall. Fig S1(b) shows the simulation cell for fluid interacting with a reflecting wall. To ensure that $P = 0.122$ in the bulk, the top wall acts as a piston that is free to move in the x and z-directions. The solid atoms in the structured walls were arranged in an fcc lattice ($\rho = 0.9\sigma^{-3}$) bonded via harmonic springs to their nearest neighbors, where the spring stiffness $k_{\text{bond}} = 5000\epsilon/\sigma^2$ and equilibrium rest length is 1.1626σ. The fluid was in contact with the $\{001\}$ face of the crystal lattice.

To minimize computational costs, we used a smaller simulation box ($\langle L_x\rangle/3 = 16.44\sigma$, $N = 2640$ fluid atoms) to evaluate the microscopic stress (see SM: Stress-Gradient Method) and LTE (see

SM: Local Thermal Equilibrium (LTE) Method) expressions. When comparing the directly computed thermo-osmotic force in the non-equilibrium simulation with the 'stress gradient' and LTE methods, we should note that the direct calculation only includes the gradient in the potential stress

$$f_x^{P,\phi}(z) = \frac{1}{\rho(z)} \left(\frac{\partial \sigma_{xx}^{\phi}(z)}{\partial T} \frac{\partial T}{\partial x} \right) \tag{8}$$

since the force computation is simply a summation over all pairwise forces. Yet, as mentioned previously, the non-uniqueness of the stress arises due to different definitions of the *potential* stress not the kinetic. Therefore, we can use our equilibrium measurements of the kinetic stress at different temperatures (see SM: Stress-Gradient Method) to calculate the gradient of the kinetic stress. Adding the kinetic contribution to our direct calculation should give the full thermo-osmotic force.

Fig 2(a, b) compare the force per particle predicted by the stress-gradient and LTE methods with those computed directly via the non-equilibrium technique. For the structured wall shown in Fig 2(b) (see Fig S3 for the Lennard-Jones surface), the non-equilibrium calculation was carried out for temperature gradients of different magnitudes in order to validate the signal. As expected, the thermo-osmotic force monotonically increases as a function of the gradient. To improve statistics, the non-equilibrium forces from the left and right regions were averaged (see Fig S2).

Surprisingly, in all cases, both the V (red) and IK (cyan) approximations of the stress gradient fail to predict the thermo-osmotic force (blue). Perhaps more significantly, the LTE approach (green) gets quite close, but still differs from the non-equilibrium result (blue). It is possible that this difference is due to deviation of the non-equilibrium result from the local thermal equilibrium approximation. Encouragingly, all methods agree in predicting zero net force in the bulk, consistent with the theory (Eq (4)).

From a mesoscopic perspective, the integral of $f_x^P(z)$ shown in Fig 2 multiplied by the corresponding density profiles $\rho(z)$ (see Fig S4(d)) yields the surface tension gradient, $\partial\gamma/\partial x$. Surprisingly, for all surfaces apart from the Lennard-Jones structured surface (see Fig S3), the mechanical and LTE approaches predict the same surface tension gradient (see Table S1). The discrepancy leads us to conclude that stress expressions fail even at a mesoscopic scale at solid-fluid interfaces (see SM: Surface Tension Gradients).

In our previous work, there was significant numerical evidence indicating that stress gradients also fail to predict microscopic Marangoni and osmotic forces due to concentration gradients [13, 14]. We have shown that near an interface, it is not possible to express the microscopic forces as the gradient of the stress tensor.

In the calculations presented in Fig 2(b), we assume that the structure of the confining solid does not depend on temperature. Symmetry then implies that, on average, a flat solid wall should exert zero net transverse force on a fluid atom. Yet, in the case of an atomically structured wall, the stress gradient predicts a non-zero force contribution from the surface (see Fig S5(c)).

To elucidate the role of the wall stress, we repeated the force calculation via the mass tensor but instead summed over only wall-fluid interactions ϕ_{wf}. Surprisingly, Fig 3(b) shows a significant force exerted by the wall on the fluid from $z = 0.8-1.4$ that scales linearly with the gradient. As a test case, the same force was measured in equilibrium simulations (blue circles) while $M_{xx} \to \infty$ where, as expected, the wall exerts no force.

To explain the wall forces shown in Fig 3(b), we consider the possibility that due to the density gradient in x induced by the thermal gradient, the average center-of-mass $x-$position (Fig 3(a)) of a fluid atom (red spheres) is asymmetric with respect to the lattice positions of the solid atoms (yellow spheres) below. Fig 3(a) shows the average $x-$position of an atom as a function of z in the equilibrium (blue circles) and non-equilibrium simulations (green, red, cyan circles).

In equilibrium, the center-of-mass position of a fluid atom in the Right region ($x = 25.48 - 48.50$ in Fig S2) is located at the region center, $x = 36.99$, also the lattice position of a solid atom. Out of equilibrium, the average position shifts away from the center in a way that scales linearly with the gradient and breaks symmetry. The force profile in Fig 3(b) is consistent with the position shift shown in Fig 3(a), since the fluid experiences a negative force where it is shifted right $z = 0.8 - 1.0$, zero force at $z = 1.075$ where there is no shift, and a small positive force where it is shifted left $z = 1.1 - 1.4$. As expected, the wall force decays extremely quickly. Surprisingly, the potential stress gradient (Fig S5(c)) predicts wall forces that are opposite in sign to the actual values and decay slowly. It is likely in the case of a purely repulsive surface (Fig 2(b)), fluid will on average be sufficiently far away such that the wall force will become exceedingly small. For the flat interface (Fig 2(a)), there are no transverse wall-fluid interactions meaning that the thermo-osmotic force is solely due to fluid-fluid interactions.

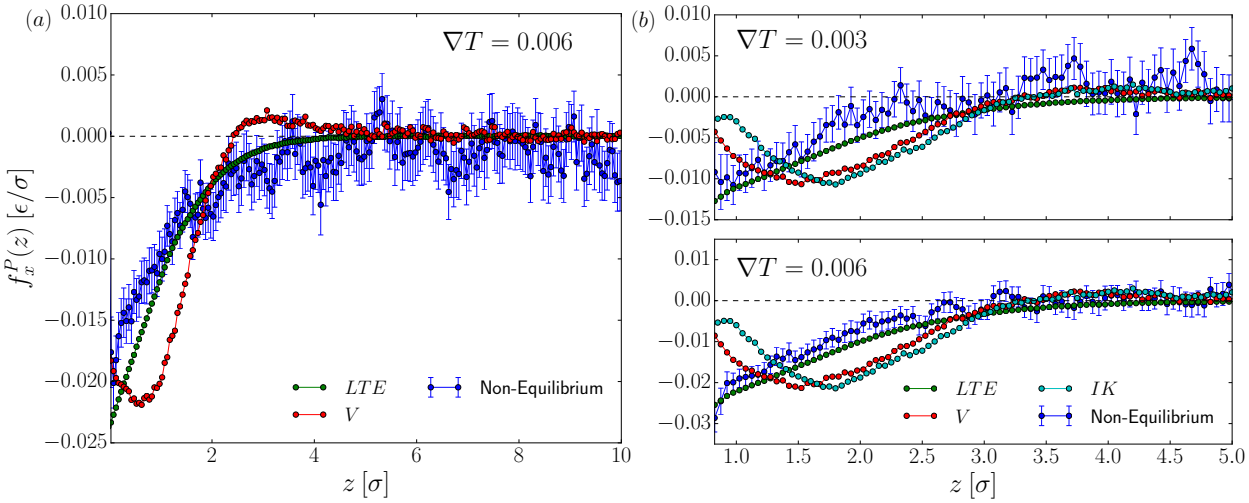

FIG. 2: Comparison of non-equilibrium force measurement (blue) with 'stress gradient' approaches using V (red) and IK (cyan) stress expressions as well as the LTE approach (green). Force profiles are plotted near (a) a flat, reflective wall and (b) a WCA wall. As the wall position is at $z = 0$, below (a) $z = 0.025$ and (b) $z = 0.825$, the local fluid density is less than 10% of the bulk density giving poor statistics.

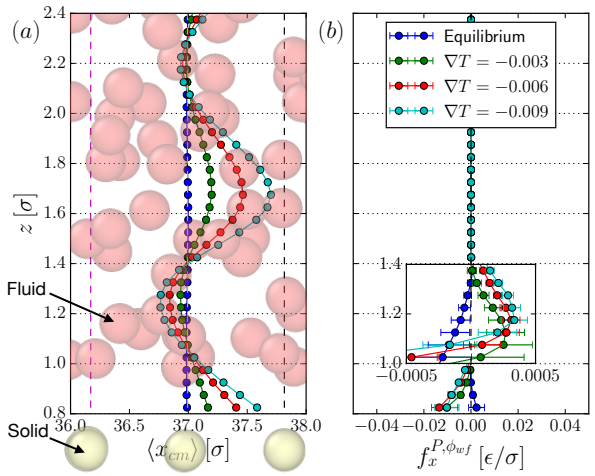

FIG. 3: (a) The average center-of-mass $\langle x_{cm} \rangle$ position of fluid atoms (red spheres) in the Right region (see Fig. S2) as a function of the height z from the surface (located at $z = 0$). (b) shows the non-equilibrium calculation of the wall force (summation of wall-fluid interactions).

In the context of existing literature, it is worth noting that Maxwell's [15] derivation of gas thermal creep flow along a solid interface approximated the surface as a reservoir behaving intermediate between a reflected and an evaporated gas. Defining the parameter f as the fraction of gas molecules absorbed and evaporated by the surface and $1 - f$ as the fraction reflected, he derived a coefficient of slipping that incorporates surface asperities. While we solely consider the case of a reflecting surface ($f = 0$, i.e. perfect slip) in Fig. 2(a), we can easily introduce partial slip by using bounce-back rules. Moreover, we can explicitly model a structured, solid surface instead of using Maxwell's approximation.

In this paper, we have reported direct calculations of the thermo-osmotic force using a non-equilibrium simulation technique. We find that near a solid-fluid interface, $f_x \neq \partial\sigma_{xx}/\partial x$ suggesting that neither the Irving-Kirkwood nor virial expression accurately predict surface forces due to temperature gradients. Although the stress is useful for a hydrodynamic description of the problem [7] it does not match with what is measured microscopically. Third, we find that an expression for the thermo-osmotic force based on the local enthalpy gets close to the true result. Finally, we have determined the contribution from wall stresses. For a structured surface, the wall structure does play a role in thermo-osmosis due to the asymmetric positioning of fluid atoms with respect to the lattice positions of solid atoms. This contribution disappears in the case of an unstructured reflecting wall.

This work was supported by the European Union grant 674979 [NANOTRANS]. We gratefully acknowledge numerous discussions with Alpha Lee, Lydéric Bocquet, Mike Cates, Patrick Warren, Ignacio Pagonabarraga and Benjamin Rotenberg. Additionally, we are grateful to Peter Wirnsberger for

helpful suggestions with the method. RG gratefully acknowledges a PhD Grant from the Sackler Fund.

* Corresponding author; df246@cam.ac.uk

[1] Lippmann, C.R. Acad. Sci. **145**, 105 (1907).
[2] Aubert, Ann. Chim. Phys. **26**, 551 (1912).
[3] D. Chretien, P. Benit, H. Ha, S. Keipert, R. El-Khoury, Y. Chang, M. Jastroch, H. Jacobs, P. Rustin, and M. Rak, bioRxiv , 133223 (2017).
[4] B. Derjaguin, N. Churaev, and V. Muller, *Surface Forces* (Plenum, New York, 1987).
[5] R. Ganti, Y. Liu, and D. Frenkel, Phys. Rev. Lett. **119**, 038002 (2017).
[6] L. Fu, S. Merabia, and L. Joly, Phys. Rev. Lett. **119**, 214501 (2017).
[7] J. Anderson, Annu. Rev. Fluid Mech. **21**, 61 (1989).
[8] P. Schofield and J. Henderson, Proc. R. Soc. A **379**, 231 (1982).
[9] J. Hansen and I. McDonald, *Theory of Simple Liquids* (Elsevier, 1990).
[10] J. Irving and J. Kirkwood, J. Chem. Phys **18**, 817 (1950).
[11] J. Weeks, D. Chandler, and H. Andersen, J. Chem. Phys **54**, 5237 (1971).
[12] S. Plimpton, J. Comput. Phys. **117**, 1 (1995).
[13] Y. Liu, R. Ganti, H. G. A. Burton, X. Zhang, W. Wang, and D. Frenkel, Phys. Rev. Lett. **119**, 224502 (2017).
[14] Y. Liu, R. Ganti, and D. Frenkel, J. Phys. Condens. Matter **30**, 205002 (2018).
[15] J. C. Maxwell, Philosophical Transactions of the royal society of London **170**, 231 (1879).